King Fahd University of Petroleum & Minerals

DEPARTMENT OF MATHEMATICAL SCIENCES

Technical Report Series

TR 069

November 1984

Sh-Waves From a Two Dimensional Source for Two Layers over a Half Space An Exact Spectral Solution and Some Numerical Results

A. Niazy and M.H. Kazi

SH-WAVES FROM A TWO DIMENSIONAL SOURCE FOR TWO LAYERS OVER A HALF-SPACE — AN EXACT SPECTRAL SOLUTION AND SOME NUMERICAL RESULTS

by

A. Niazy* and M. H. Kazi**

ABSTRACT

In this paper we present an exact spectral solution for the two-dimensional, anti-plane, shear wave motion due to a line-source located at the top-surface in a structure consisting of two uniform layers overlying a uniform half-space. We explain the difficulties inherent in the application of the discrete-wavenumber method of Bouchon and Aki (1977) to compute the solution numerically in the range of frequencies which are of interest in exploration seismology and propose an alternative procedure. Synthetic seismograms at three different near source stations located at equal distances from each other are obtained from the Fourier digital synthesis of the exact spectral representations of the seismic displacement. The results indicate the presence of an evanescent plane wave which travels vertically up and down and decays exponentially with distance from the source, and show all other physically interesting events that are expected in the record.

---

* Department of Earth Sciences,
University of Petroleum and Minerals, Dhahran, Saudi Arabia.

** Department of Mathematical Sciences,
University of Petroleum and Minerals, Dhahran, Saudi Arabia.

INTRODUCTION

The advantages of using shear waves have long been realized in seismic exploration because shear waves are less sensitive to the fluid content and should give better indication of the engineering properties of the matrix (see Johnson (1979)). However, early attempts to use shear waves in exploration seismology were frustrated by the inability to generate shear waves efficiently. This difficulty was later circumvented with the invention of vibroseis trucks which made it possible to generate shear waves efficiently by using horizontal surface vibrators. The motivation to use shear waves lead naturally to three component recording because most of the energy in reflected shear waves resides in the horizontal components of motion.

Niazy (1975) adapted a three component statistical polarization filter discussed by Montalbetti and Kanasewich (1970) to enhance reflected events and successfully suppressed Rayleigh waves. During the synthesis of the filter, the direction cosines of the incident wavelet are computed. This is expected to lead to significant improvements even on conventional 3-D migration schemes, provided that the type of the wavelet is properly identified. Unfortunately, the developed polarization filter could not discriminate against Love waves, as they had the same polarization characteristics as reflected shear waves. In order to overcome this difficulty it is necessary to have closer understanding of the problems involving shear wave motion.

In this paper we consider the two-dimensional problem of propagation of anti-plane shear waves due to a line-source through a simplified earth model consisting of two uniform layers overlying a half-space. Figure 1 shows the geometry and elastic parameters of the problem. The surface layer in this model represents the troublesome weathered layer on the surface of the earth. The lower interface corresponds to a deep reflector. The source is a line-force in the y-direction acting at the origin. Because the source is at the surface (as it is usually in exploration) the Love wave motion reaching the receiver is expected to be high in frequency so that we cannot discriminate against them by using a band-pass filter. Furthermore, because Love waves have slower velocities than β_2(See Figure 1) they may very well reach the receiver at the same time as the shear waves reflected from the lower interface. As we mentioned before, Love waves will have the same polarization as the reflected shear waves with similar frequency content. However, we may be able to get rid of the undesired Love wave portion by recording at sufficiently close distances on the ground so that we can take the spatial Fourier Transform of the records and we may then multiply by a spatial notch filter and then go back to space and time domain to recover the filtered trace at each station. In order to accomplish this, we find it expedient to obtain an exact solution for the impulse response of the medium at a station located on the surface. In this paper we present an exact spectral solution of the problem, analytically and construct the synthetic seismograms for the model show in Figure 1. The time records are obtained from the Fourier digital synthesis of the exact spectral representation of the seismic displacement. We show the spectra corresponding to the time records for stations located at $x = .2, .3$ and $.4$ km and discuss their corresponding time traces.

FIG. 1

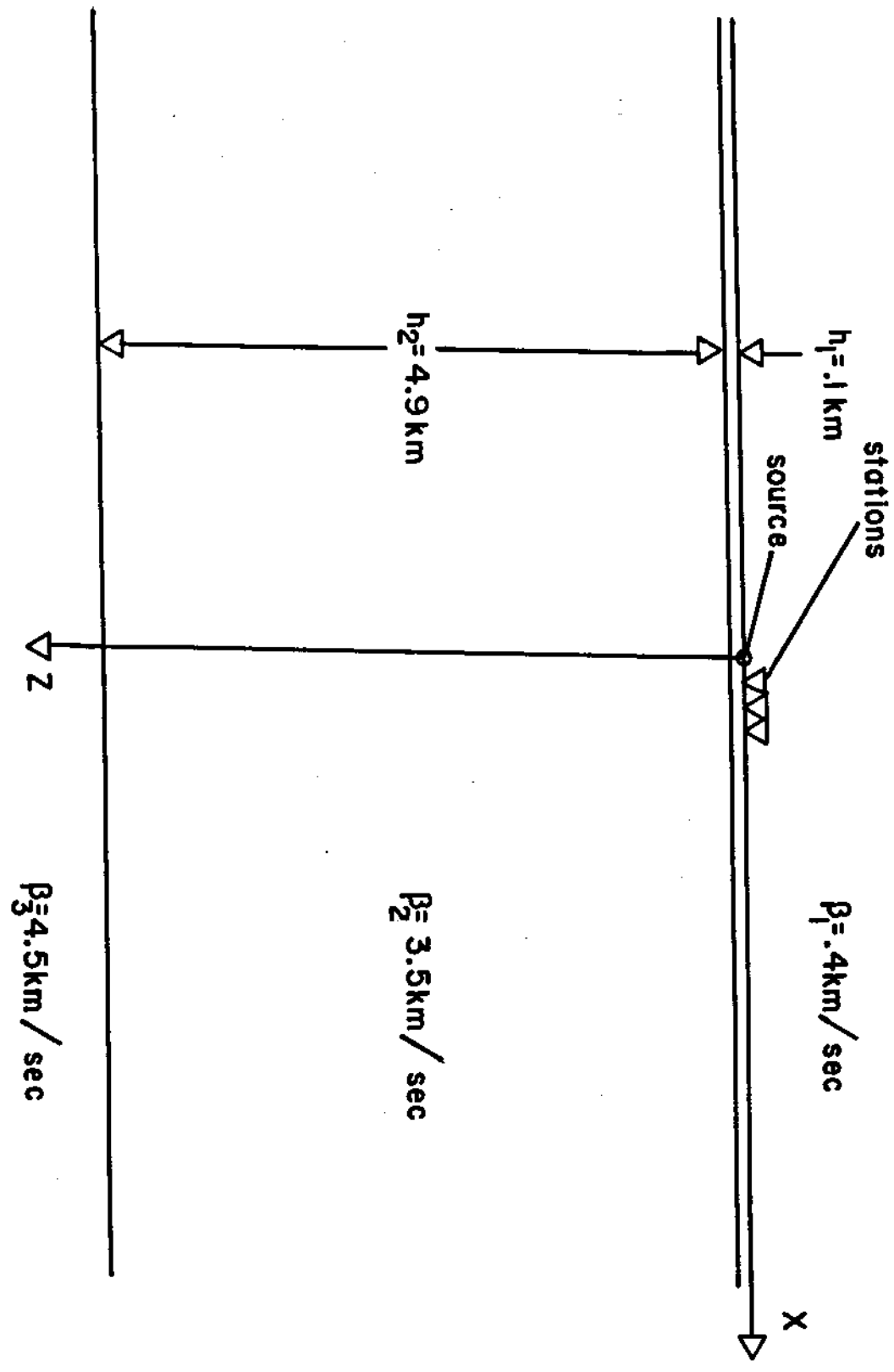
stations
source
h_1= .1 km
h_2= 4.9 km
Z
X
β_1= .4km/ sec
β_2= 3.5km/ sec
β_3=4.5km/ sec

Fig. 1

Basic Equations

We consider anti-plane, two dimensional shear wave motion due to a line-source located at the top-surface in the model shown in Figure 1. Let ψ be the rotational potential, τ_{yz} be the yz-component of the shear stress and v be the y-component of the anti-plane displacement. Then for a steady-state source, we have

$$v = -\frac{\partial \psi}{\partial x} \tag{1}$$

$$\tau_{yz} = -\mu \frac{\partial^2 \psi}{\partial x \partial z} \tag{2}$$

In region I, the shear-wear potential can be written as:

$$\psi_I = \psi_1 e^{-ikx-\nu_{\beta_1} z+i\omega t} + \psi_2 e^{-ikx+\nu_{\beta_1} z+i\omega t} \tag{3}$$

where ψ_1 and ψ_2 are independent of x and z and $\nu_{\beta_1} = i(\frac{\omega^2}{\beta_1^2} - k^2)^{\frac{1}{2}}$.

The first term represents down-going waves and the second term represents up-going waves. Both terms satisfy the wave equation

$$\frac{\partial^2 \psi}{\partial t^2} = \beta^2 \nabla^2 \psi \quad , \quad \nabla^2 = \frac{\partial^2}{\partial x^2} + \frac{\partial^2}{\partial z^2} \tag{4}$$

Similarly, in regions II & III the potentials are given by

$$\psi_{II} = \psi_3 e^{-ikx-z\nu_{\beta_2}+i\omega t} + \psi_4 e^{-ikx+z\nu_{\beta_2}+i\omega t} \tag{5}$$

$$\psi_{III} = \psi_5 e^{-ikx-z\nu_{\beta_3}+i\omega t} \tag{6}$$

We have the following boundary conditions to satisfy:

$$\tau_{yz}\Big|_{z=0} = Ye^{i\omega t-ikx} \tag{7}$$

$$v_I\Big|_{z=z_1} = v_{II}\Big|_{z=z_1} \tag{8}$$

$$v_{II}\Big|_{z=z_2} = v_{III}\Big|_{z=z_2} \tag{9}$$

$$\tau^{I}_{yz}\Big|_{z=z_1} = \tau^{II}_{yz}\Big|_{z=z_1} \tag{10}$$

$$\tau^{II}_{yz}\Big|_{z=z_2} = \tau^{III}_{yz}\Big|_{z=z_2} \tag{11}$$

where we assumed a load distribution on the surface of the form $Ye^{i\omega t-ikx}$ as indicated by equation (4). In these equations the Roman subscripts and superscripts indicate the quantity in the corresponding region as shown in Figure 1.

Exact Solutions

Substituting from (1), (2), (3), (5) and (6) in equations (7), (8), (9), (10) and (11), we get five equations in the five unknowns ψ_1, ψ_2, ψ_3, ψ_4, and ψ_5, which we can solve and get the expressions for ψ_1 and ψ_2. The equations are given by

$$\psi_1 - \psi_2 = \frac{iY}{\mu_1 k \nu_{\beta_1}} \tag{12}$$

$$\psi_1 e^{-\nu_{\beta_1} z_1} + \psi_2 e^{\nu_{\beta_1} z_1} - \psi_3 e^{-\nu_{\beta_2} z_1} - \psi_4 e^{\nu_{\beta_2} z_1} = 0 \tag{13}$$

$$\psi_1 \mu_1 \nu_{\beta_1} e^{-\nu_{\beta_1} z_1} - \psi_2 \mu_1 \nu_{\beta_1} e^{\nu_{\beta_1} z_1} - \psi_3 \mu_2 \nu_{\beta_2} e^{-\nu_{\beta_2} z_1} + \psi_4 \mu_2 \nu_{\beta_2} e^{\nu_{\beta_2} z_1} = 0 \tag{14}$$

$$\psi_3 e^{-\nu_{\beta_2} z_2} + \psi_4 e^{\nu_{\beta_2} z_2} - \psi_5 e^{-z_2 \nu_{\beta_3}} = 0 \tag{15}$$

$$\psi_3 \mu_2 \nu_{\beta_2} e^{-\nu_{\beta_2} z_2} - \psi_4 \mu_2 \nu_{\beta_2} e^{\nu_{\beta_2} z_2} - \psi_5 \nu_{\beta_3} \mu_3 e^{-z_2 \nu_{\beta_3}} = 0 \tag{16}$$

Solving (12) - (16) for ψ_1 and ψ_2, we get after considerable effort:

$$\psi_1 = \frac{iYe^{\nu_{\beta_1} z_1}}{4\mu_1 k \nu_{\beta_1}} \frac{[e^{\nu_{\beta_2}(z_2 - z_1)}(\nu_{\beta_2} + \nu_{\beta_1})(\nu_{\beta_2} + \nu_{\beta_3}) - e^{-\nu_{\beta_2}(z_2 - z_1)}(\nu_{\beta_2} - \nu_{\beta_1})(\nu_{\beta_2} - \nu_{\beta_3})]}{[\nu_{\beta_2}^2 \cosh(\nu_{\beta_1} z_1)\sinh(\nu_{\beta_2}(z_2 - z_1)) + \nu_{\beta_2}\nu_{\beta_3}\cosh(\nu_{\beta_1} z_1)\cosh(\nu_{\beta_2}(z_2 - z_1))]} \tag{17}$$

$$\psi_1 = \frac{iYe^{-\nu_{\beta_1} z_1}}{4\mu_1 k\nu_{\beta_1}} \frac{[(\nu_{\beta_1}-\nu_{\beta_2})(\nu_{\beta_3}+\nu_{\beta_2})e^{\nu_{\beta_2}(z_2-z_1)} + (\nu_{\beta_1}+\nu_{\beta_2})(\nu_{\beta_2}-\nu_{\beta_3})e^{-\nu_{\beta_2}(z_2-z_1)}]}{[\nu_{\beta_2}^2 \cosh\nu_{\beta_1} z_1 \sinh(\nu_{\beta_2}(z_2-z_1)) + \nu_{\beta_2}\nu_{\beta_3}\cosh(\nu_{\beta_1} z_1)\cosh(\nu_{\beta_2}(z_2-z_1))]} \tag{18}$$

The displacement at the surface is given by

$$V\Big|_{z=0} = \frac{-\partial\psi}{\partial x}\Big|_{z=0} = ike^{i\omega t - ikx}[\psi_1+\psi_2]$$

We are seeking the solution for a source of the form $\delta(x)\delta(t)$ at the origin in Figure 1. The solution for such a source is then given by

$$v_\delta(x,0,t) = \frac{1}{(2\pi)^2}\int_{-\infty}^{\infty}\int_{-\infty}^{\infty} v(\omega,k,x)e^{-ikx+i\omega t}\,dk\,d\omega \tag{19}$$

If v were a rational function of $\omega, k, \nu_{\beta_1}, \nu_{\beta_2}$, and ν_{β_3}, then we could hope to apply Cagniard's method by looking for a transformation that would put integral $\tilde{v}(x,0,k,t) = \frac{1}{2\pi}\int_{-\infty}^{\infty} v(\omega,k,x)e^{i\omega t - ikx}\,d\omega$ in the form

$$p^n \int_0^\infty g(\tau)e^{-p\tau}\,d\tau\ ,\quad p > 0,$$

wherefrom $g(\tau)$ is recognized as the impulse response or one of its derivaties or indefinite integrals depending on the value of n (see Niazy (1974)).

Since in our case the denominator involves transcendental functions such an approach does not seem feasible.

We next attempted a direct application of the discrete-wavenumber method proposed by Bouchon & Aki (1977) for simple media. Under that method, the steady state solution is computed and from it the impulse response is computed numerically by using the Fast Fourier Transform algorithm.

To apply the discrete-wavenumber method we assume that the source is repeated periodically with period L along the x-axis. We choose L sufficiently large so that only the source at the origin contributes to the record during the time interval of interest. We can then write the steady-state solution:

$$u_\delta = \frac{-4\pi Y}{L\mu_1} e^{i\omega t} \sum_{n=0}^{\infty} \cos k_n x [\mu_2^2\nu_2^2 \sinh z_1\nu_1 \sinh\nu_2\Delta z + \mu_2\mu_3 \sinh\nu_1 z_1 \cosh(\Delta z\nu_2)\nu_2\nu_3 +$$

$$\mu_1\mu_2\nu_1\nu_2 \cosh z_1\nu_1 \cosh\Delta z\nu_2 + \mu_1\mu_3\nu_1\nu_3 \sinh\Delta z\nu_2 \cosh z_1\nu_1]/[\nu_1\{\mu_2^2\nu_2^2 \cosh\nu_1 z_1 \sinh\nu_2\Delta z$$

$$+\mu_2\mu_3\nu_2\nu_3 \cosh\nu_1 z_1 \cosh\nu_2\Delta z + \mu_1\mu_2\nu_1\nu_2 \sinh\nu_1 z_1 \cosh\nu_2\Delta z + \mu_1\mu_3\nu_1\nu_3 \sinh\nu_1 z_1 \sinh\nu_2\Delta z\}] \qquad (20)$$

where $k_n = \frac{2\pi n}{L}$, $\nu_m = \sqrt{k_n^2 - \frac{\omega^2}{\beta_m^2}}$, $m = 1,2,3, \Delta z = z_2 - z_1$.

We choose the following model parameters to cover a case of interest to us in seismic exploration:

$\beta_1 = .4$ km/sec , $\beta_2 = 3.5$ km/sec, $\beta_3 = 4.5$ km/sec

$z_1 = .1$ km , $z_2 = 5$ km, 10 Hz $\leq$ frequency $\leq$ 100 Hz

We then require a time record of $\simeq$ 3.7 sec to sample the reflected arrival from the deep interface.

In the limit as $n \to \infty$, the series in (20) behaves like $\frac{\cos k_n x}{k_n}$ which implies slow convergence of the series. Choosing a reasonable value for L say about 12 km, we found that for certain frequencies the series has not convered to an accuracy of five significant figures even after summing 10^5 terms, indicating that a straightforward application of the method is not practical.

The reason for this slow convergence in contrast to the applications of Bouchon (1977), Bouchon (1980) and Bouchon & Aki (1980) is that the source and the receiver are both at the same level namely the surface of the earth, thereby eliminating the exponential damping factor of the form $e^{-h\nu_\beta}$ (h being the vertical separation between the source level and the receiver level) that is present in the above-mentioned application. This suggests putting the source for example at a small depth h for convenience of calculation. However, it will be difficult to esimate the error caused by such a procedure knowing that convergence problems arise when h is too small. Unfortunately, the relative source-receiver location at the free-surface is of primary interest in exploration seismology. Consequently, an exact treatment of the problem is desirable. Once the results are obtained, one can then investigate the effect of putting the source at a small depth using the discrete-wavenumber method and compare the resulting solution with the exact solution.

FIG. 2

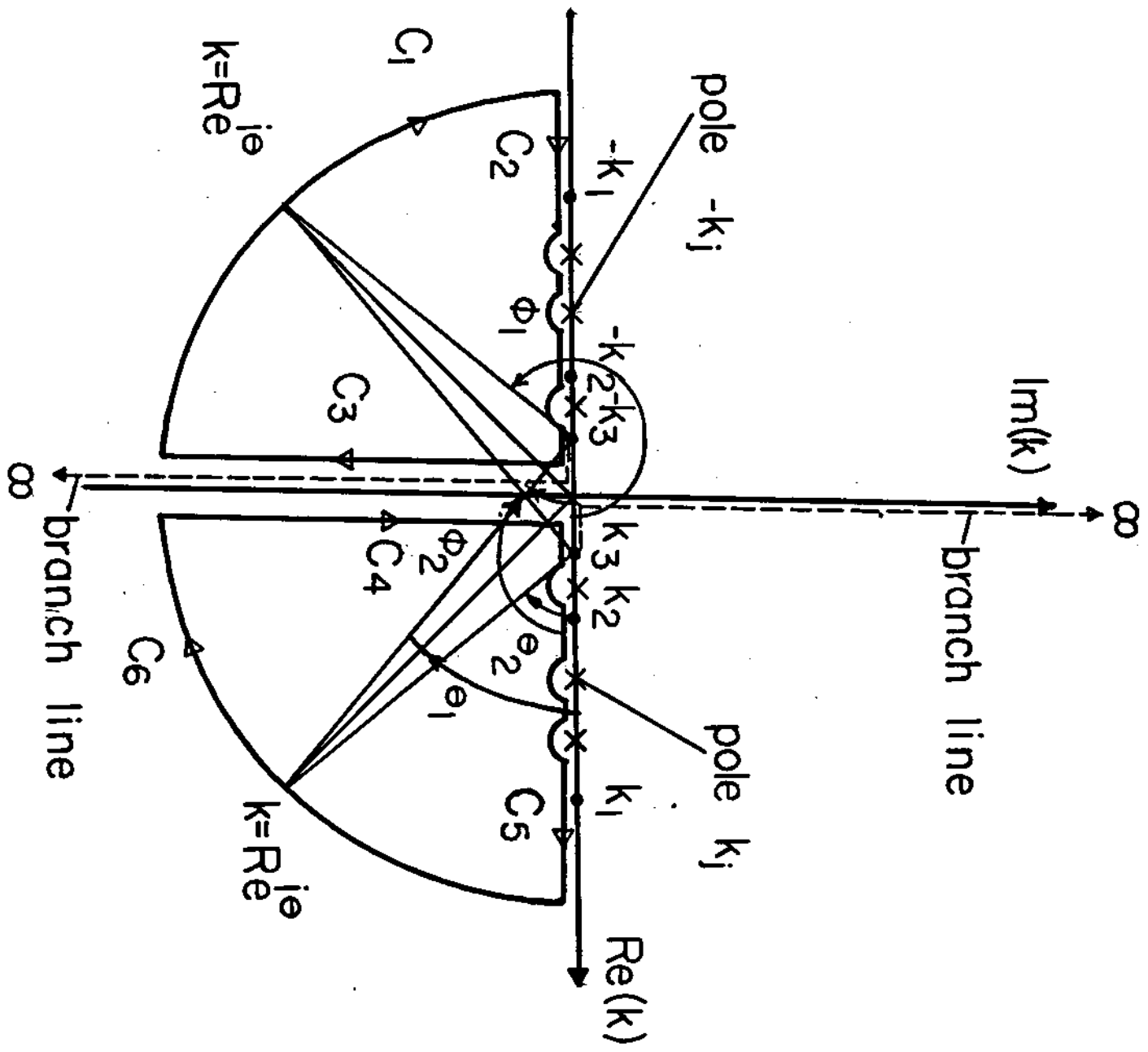
C1
C2
C3
C4
C5
C6
k=Re^ie
k=Re^ie
-k1
-k2-k3
k3 k2
k1
pole -kj
pole kj
Φ1
Φ2
e1
e2
∞
∞
branch line
branch line
Im(k)
Re(k)

We go now to the integral formulation of the problem. The solution can be written as:

$$u_\delta = \frac{-Ye^{i\omega t}}{2\pi\mu_1}\int_{-\infty}^{\infty} e^{-ikx}[\mu_2^2\nu_2^2\sinh z_1\nu_1\sinh\Delta z\nu_2+\mu_2\mu_3\sinh z_1\nu_1\cosh(\Delta z\nu_2)\nu_2\nu_3+$$

$$\mu_1\mu_2\nu_1\nu_2\cosh z_1\nu_1\cosh\Delta z\nu_2+\mu_1\mu_3\nu_1\nu_3\sinh\Delta z\nu_2\cosh z_1\nu_1] +$$

$$[\nu_1\{\mu_2^2\nu_2^2\cosh\nu_1 z_1\sinh\nu_2\Delta z+\mu_2\mu_3\nu_2\nu_3\cosh\nu_1 z_1\cosh\nu_2\Delta z +$$

$$\mu_1\mu_2\nu_1\nu_2\sinh\nu_1 z_1\cosh\nu_2\Delta z+\mu_1\mu_3\nu_1\nu_3\sinh\nu_1 z_1\sinh\nu_2\Delta z\ ] \qquad (21)$$

The above integral is of the form $\int_{-\infty}^{\infty} f(k_1\nu_1,\nu_2,\nu_3)e^{-ikx}dk$ where $f = \frac{g(k)/\nu_1}{h(k)}$.

We note that $f(k,-\nu_1,\nu_2,\nu_3) = f(k,\nu_1,\nu_2,\nu_3)$ and $f(k,\nu_1,-\nu_2,\nu_3) = f(k,\nu_1,\nu_2,\nu_3)$ which means that k_1 and k_2 are not branch points ($k_m = \frac{\omega}{\beta_m}$, m = 1,2,3). However, $f(k,\nu_1,\nu_2,-\nu_3) \neq f(k,\nu_1,\nu_2,\nu_3)$ and hence k_3 is a branch point.

We now consider the integral in the complex k-plane with the requirement that $Re\nu_3 > 0$ (i.e., no incoming waves from infinity). We choose our branch cut at $Re\cdot(\nu_3) = 0$ as indicated in Figure 2.

Without loss of generality we choose $x > 0$ (because of the physical symmetry with respect to x). We consider integration on $C_1+C_2+C_3$ and

on $C_4+C_5+C_6$ separately. We note that $|f(k)| \to 0$ as $|k| \to \infty$ in the lower half plane. The poles of f are in the intervals $|k| \epsilon (k_3, k_1)$, Re $(\nu_3) > 0$. In quadrant III we have $\pi < \phi_1 < 2\pi$, $-\pi < \phi_2 < \frac{-\pi}{2}$ and $0 < \frac{\phi_1+\phi_2}{2} < \frac{\pi}{2}$ satisfying the requirement that Re $(\nu_3) > 0$.

Similarly in IV, $\frac{-\pi}{2} < \theta_1 < 0$, $-\pi < \theta_2 < 0$, $\frac{-\pi}{2} < \frac{\theta_1+\theta_2}{2} < 0$ and Re $(\nu_3) > 0$.

We consider now $I_1 = \lim_{R\to\infty} \int_{C_1+C_2+C_3} e^{-ikx} f \, dk$.

On C_1, $\int_{C_1} e^{-ikx} f(k) dk \to 0$ as $R \to \infty$ by Jordan's Lemma

$$\therefore \quad I_1 = -\pi i \sum_{j=1}^{N} \text{Res}(e^{-ikx} f(k), k_j) \quad \text{where } k_j < 0 \text{ and } h(k_j) = 0$$

N = number of modes present at ω

$$= \int_{C_2} e^{-ikx} f \, dk + \int_{C_3} e^{-ikx} f \, dk$$

$$\therefore \quad \int_{C_2} e^{-ikx} f \, dk = -\pi i \, S_1 - \int_{C_3} f(k) e^{-ikx} dk, \quad S_1 = \text{sum of the residues.}$$

On C_3, $k = iy$, $e^{-ikx} = e^{xy}$ for $-\infty < y < 0$, $\nu_3 = \sqrt{k_3^2+y^2} e^{i\pi/2}$. The integral $\int_{C_3} e^{-ikx} f(k) dk$ is rapidly convergent because $|f(k)| \sim \frac{1}{|k|}$ as $|k| \to \infty$ and can be evaluated numerically to arbitrary precision.

Similarly, $\int_{C_5} \bar{e}^{ikx} f(k)dk = -\pi i \sum_{m=1}^{N} \text{Res}(\bar{e}^{ikx} f(k), k_m) - \int_{C_4} \bar{e}^{ikx} f(k)dk$, $k_m > 0$.

On C_4, $k = iy$, $\bar{e}^{ikx} = e^{xy}$, $-\infty < y < 0$, $\nu_{\beta_3} = \sqrt{k_3^2+y^2}\ \bar{e}^{i\pi/2}$ and $\int_{C_4} \bar{e}^{ikx} f(k)dk$ is a rapidly convergent integral and can be evaluated numerically to arbitrary precision.

$$\bar{e}^{i\omega t} A u_\delta = \int_{-\infty}^{\infty} \bar{e}^{ikx} f(k)dk = -\pi i \sum_{J=1}^{N} \text{Res}\cdot[f(k)\bar{e}^{kxi}, k_j] + \text{Res}\cdot[f(k)\bar{e}^{ikx}, -k_j],$$

$$-\int_{0}^{-\infty} e^{xy} f(iy, \nu_{\beta_3} = i\sqrt{k_3^2+y^2})idy - \int_{-\infty}^{0} e^{xy} f(iy, \nu_{\beta_3} = -i\sqrt{k_3^2+y^2})idy, \tag{22}$$

where $A = \frac{-2\pi\mu_1}{\gamma}$.

Thus, at any angular frequency ω, we have to determine the number of modes N, compute the poles $\mp k_j$ and the Residue contributions from all poles and carry out the numerical integration to get the spectral displacement u_δ which can be numerically integrated by using the Fast Fourier Transform to get the time record for any source time function of interest.

Numerical Results and Discussion

Appendix II gives the discussion of the poles of $f(k)$ in (22) and the details of the method of evaluating them. Briefly, at each value of ω, we computed the Love poles for the problem of a layer over a half-

space, with the properties of the layer being the same as that of the surface layer in our model, and the properties of the half-space corresponding to those of the second (thick) layer in our model. We then used each such pole as an initial approximation to the Newton-Raphson method to compute the pole of the dispersion function for our model. As the integrand f is in the form of the ratio of two functions, we had to verify that the zeros of the numerator were not zeros of the denominator, and that the obtained zeros were all the zeros of the denominator.

As for the other two integrals, they reduced to the evaluation of an integral of the form

$$\int_{0}^{-\infty} v(y)e^{+xy}\,dy, \quad v(y) < 0$$

We chose an upper limit of inegration-L such that $(\frac{v(-L)e^{-xL}}{v(0)}) < 10^{-16}$ (double precision arithmetic in IBM machines).

A straightforward integration proved to be extremely slowly convergent. An attempt to use Romberg Integration as given in the IBM Scientific Subroutine Package, proved fruitless as for practically all frequencies of interest the subroutine gave an error message indicating failure to converge. The cause of the problem was that the integrand varies rapidly over a limited part of its domain. An alternative proved to be successful was to divide the integration interval (0,-L) into 2^m intervals. We then apply Romberg Integration to each interval and sum the individual contributions. If the integration scheme fails to converge over any of the

intervals, we increase m by one and repeat the process, until the scheme succeeds in evaluating the integral to the desired precision.

The contributions to the spectra from the residue terms and from the branch line terms are computed separately. Figure 3 shows the contribution from the residue terms plotted as a function of frequency for x = .2, .3, .4 km. All graphs are plotted to the same scale. The lower plot corresponds to x = .2 km. We notice the substantial increase in the jaggedness in the spectrum as x increases, which necessitated a very fine sampling of the function namely 2048 points for each graph. The sampling interval is $\frac{1}{20.48}$ Hz. Because the time function is real, this procedure allows us to double the number of sample points in the frequency domain as the values for negative frequencies are simply the complex conjugate of the values for positive frequencies. This increase in jaggedness with distance is what made the method impractical for the computation of the records at larger distance.

Figure 4 shows the integral contributions to the spectra corresponding to those shown in Figure 3. Figure 5 shows the sum of the two contributions also plotted for x = .2, .3, and .4 km.

Figure 6, Figure 7 and Figure 8 show the relative amplitude of the two kinds of terms and their sum for x = .2 km, .3 km and .4 km respectively. We will discuss the physical meaning of the two terms when we discuss the time displacement records corresponding to them.

Next we consider the time records corresponding to the spectra that we have just discussed. Figure 9 shows the time records corresponding to the spectra in Figure 3. The most dominant pulses on the records correspond to multiple reflections of the primary pulse. Figure 15 shows the geometry for some of the multiples and some of the important phases that are of interest in our records. Table 1 in Appendix I gives the arrival times for the various phases at the different stations. The time records were obtained from the spectra by digital Fourier Synthesis as outlined in Appendix I. The time sampling interval is 5 msec. and number of samples in each record is 1500 samples.

Figure 10 shows the time records corresponding to the spectra shown in Figure 4. They correspond to the branch-line integrals' contributions. The figure shows basically a multiply reflected evanescent plane wave (decaying exponentially with distance from the source) propagating vertically up and down and changing polarity at each reflection. Although this wave seems to violate casuality as it seems to reach all receivers at the same time, this is a consequence of its being an inhomogeneous plane wave travelling vertically up and down and therefore it has an infinite apparent velocity. The violation of casuality may be a consequence of the fact that apparent velocity of the wave is so large that the difference in its interval time between the three stations under consideration is less than the sampling interval. In fact Table 1 shows that this is the case for the reflection of interest coming from the deeper interface (Appendix I).

Figure 11 shows the time records which are the sum of those shown in Figure 10 and Figure 9; clearly, the branch-line integral contribution while small, is not insignificant. Figures 12, 13 and 14 show the relative amplitude of the two contributions relative to their sum for all three stations.

The event of most interest to us is the deep reflection from the deeper interface. From the examination of the last three figures, it is clear that the event, if it is there, is too small to be visible on such unprocessed plots. We will apply two standard techniques used in the seismic exploration for oil. The first technique is clipping. Let $f(t)$ be the seismic trace of interest. Let f_{max} be the maximum absolute value of the trace of interest. We define $f(t)$ by:

$$f(t) = \left\{ \begin{array}{ll} f(t) & \text{if } |f(t)| < \alpha f_{max} \\ \alpha f_{max} \text{ Sign } (f(t)) & \text{if } |f(t)| \geq \alpha f_{max} \end{array} \right\}, \quad 0 < \alpha < 1$$

In our case we take $\alpha = .05$. We follow the clipping by applying Automatic Gain Control to the trace defined as follows. Let $g(t)$ be the clipped trace, t is the sampling interval and let N be the Gain Control window.

We define $$|\bar{g}(\Delta tm)| = \frac{1}{N} \sum_{j=m-\frac{N}{2}}^{m+\frac{N}{2}} |g(j\Delta t)|$$

We then define $$\tilde{g}(m\Delta t) = A \frac{g(m\Delta t)}{|\bar{g}(m\Delta t)|}$$ where A is a constant.

$$|\bar{g}(0)| = \frac{1}{N} \sum_{j=0}^{N} |g(j\Delta t)| \quad \text{and}$$

$$|\bar{g}(M)| = \frac{1}{N} \sum_{j=M-N}^{M} |g(j\Delta t)| \quad , \text{where } g(M) \text{ is the last sample.}$$

This has the effect of giving us a record with the same mean amplitude A (over the sampling window N) for the entire record. In our case, we chose $N = 31$ and $A = 100$.

Figure 16 shows the results of applying the two techniques consecutively to the traces show in Figure 10. We have indicated above the time axis the location of the major events shown in Table 7 for the station at x = .2 km. The time locations for the major events at the other stations may be found by the aid of Table 1, noting that .4 sec is equivalent to .5 cm. on the time axis. We clearly see now the deep reflection denoted by Ro and we see its multiples in the surface layer denoted by R_1, R_2, R_3..... As the wave reflected from the deeper interface travelled a very long distance, more than 10 km, it arrives at the surface layer almost as a plane wave.

Because the separation between the source and stations is small compared to the depth of the reflecting interface, the angle of incidence is almost normal and the difference in the arrival time between the three stations is within one sample interval. The amplitude of the wave is so small because of two factors. The first factor is the long distance that

it has to travel. The second factor is the large impedence contrast between the surface layer and the intermediate layer which allows only a small fraction of the energy to penetrate to the deeper medium and enhance the multiple reflections within the surface layer.

Acknowledgements

This work has been done as a part of research project No. (AR-3-032) sanctioned by Saudi Arabian National Centre for Science and Technology (SANCST). The authors acknowledge the SANCST support with thanks.

References

Aki, K., and Richards, P.G., 1980. Quantitative seismology, V.1, p.262-265: San Francisco, W.H. Freeman and Company.

Bouchon, M., and Aki, K., 1977. Discrete wave number representation of seismic - source wave fields: Bull. Seism. Soc. Am. V. 67, p. 259-277.

Bouchon, M., 1980. The motion of the ground during an earthquake, Part I: the case of a strike-slip fault: J. Geophys. Res. V. 85, p. 356-366.

Bouchon, M., and Aki, K., 1980. Simulation of Long-period near-field motion for the great California earthquake of 1857: Bull. Seism. Soc. Am. V. 70, p. 1669-1682.

Johnson, W.E., 1979. Relationship between shear wave velocities and geotechnical parameters: Geophysics, V. 44, p. 364.

Motalbetti, J.F., and Kanasewich, E.R., 1970. Enhancement of teleseismic body phases with a polarization filter: Geophys. J. Roy. Astr. Soc. V. 21, p. 119-129.

Niazy, A., 1974. An exact solution for a finite moving dislocation in the elastic half-space with application to the San Fernando earthquake of 1971: Ph. D. thesis submitted to M.I.T.

Niazy, A., 1975. 3-D polarization filter, Technical Memo, Chevron Oil Field Research Company.

Pilant, W.L., 1979. Elastic waves in the earth: Elsevier, New York, p. 195-196.

Appendix I

Figures and Figure Captions

FIG. 1 : Geometry and material constants for the wave propagation problem under consideration. The source is a line-force acting normal to the plane of the figure and the displacement is also antiplane. The densities are:

$\rho_1 = 2.4 gm/cm^3$, $\rho_2 = 2.6 gm/cm^3$ and $\rho_3 = 2.7 gm/cm^3$

FIG. 2 : The contour of integration.

FIG. 3 : The residues' contribution to the spectrum plotted as a function of frequency (in Hz) for $x = .2$ km (lower curve), .3 km and .4 km. Sampling interval is $\frac{1}{20.48}$ Hz, and the number of samples is 2048.

FIG. 4 : The branch-line integrals' contribution to the spectrum, with the same choices as those of FIG. 3.

FIG. 5 : The total spectrum (sum of the records in FIG. 3 & FIG. 4)

FIG. 6 : The residues' contribution (lower curve), branch line integrals' contribution (middle curve) and their sum plotted to the same scales for $x = .2$ km.

FIG. 7 : Frequency records corresponding to FIG. 6 but with $x = .3$ km.

FIG. 8 : Frequency records corresponding to FIG. 6 but with $x = .4$ km.

FIG. 9 : Time records corresponding to frequency records shown in FIG. 3.

FIG. 10 : Time records corresponding to frequency records shown in FIG. 4.

FIG. 11 : Time records corresponding to frequency records shown in FIG. 5.

FIG. 12 : Time records corresponding to frequency records shown in FIG. 6.

FIG. 13 : Time records corresponding to frequency records shown in FIG. 7.

FIG. 14 : Time records corresponding to frequency records shown in FIG. 8.

FIG. 15 : Some of the important phases shown in Fig. 16.

FIG. 16 : Complete time records after clipping and after applying the Automatric Gain Control. Lower trace is for $x = .2$ km, middle trace is for $x = .3$ km., and upper trace for $x = .4$ km. Arrival times for the important phases for $x = .2$ km are indicated by arrows on the time axis.

Appendix II

Poles of the Integrand in Equation (22) and their Residue Contributions

The integrand in equation (22) is of the form :

$$F(w,k) = \frac{f(w,k)}{\nu_1 g(w,k)} \quad \text{where} \quad \nu_n = \sqrt{k^2 - \frac{w^2}{\beta_n^2}} \quad \text{and,}$$

$$f(w,k) = \mu_2^2\nu_2^2 \sinh z_1\nu_1 \sinh \Delta z\nu_2 + \mu_2\mu_3 \sinh z_1\nu_1 \cosh(\Delta z\nu_2)\nu_2\nu_3 +$$

$$\mu_1\mu_2\nu_1\nu_2 \cosh z_1\nu_1 \cosh \Delta z\nu_2 + \mu_1\mu_3\nu_1\nu_3 \sinh \Delta z\nu_2 \cosh z_1\nu_1$$

$$g(w,k) = \mu_2^2\nu_2^2 \cosh \nu_1 z_1 \sinh \nu_2 \Delta z + \mu_2\mu_3\nu_2\nu_3 \cosh \nu_1 z_1 \cosh \nu_2 \Delta z +$$

$$\mu_1\mu_2\nu_1\nu_2 \sinh \nu_1 z_1 \cos \nu_2 \Delta z + \mu_1\mu_3\nu_1\nu_3 \sinh \nu_1 z_1 \sinh \nu_2 \Delta z.$$

The poles of F are the zeros of g provided that f does not have zeros at the same points as g. For any given value of w, we keep w fixed and try to solve for the zeros of f and g.

a) Zeros of g:

Case 1: $\beta_1 < c < \beta_2$, $c = \frac{w}{k}$

$$\therefore \quad \nu_1 = iw\gamma_1, \gamma_1 = \sqrt{\frac{1}{\beta_1^2} - \frac{1}{c^2}} \quad , \quad \nu_2 = w\gamma_2, \gamma_2 = \sqrt{\frac{1}{c^2} - \frac{1}{\beta_2^2}}$$

$$\nu_3 = w\gamma_3, \gamma_3 \sqrt{\frac{1}{c^2} - \frac{1}{\beta_3^2}}$$

$$\therefore \quad g(w,k) = \mu_2^2\nu_2^2 \cos wz_1\gamma_1 \sinh \nu_2\Delta z + \mu_2\mu_3\nu_2\nu_3 \cos w_1 z_1\gamma_1 \cosh\nu_2\Delta z +$$

$$\mu_1\mu_2\nu_1\nu_2 i \sin wz_1\gamma_1 \cosh\nu_2\Delta z + \mu_1\mu_3\nu_1\nu_3 i \sin wz_1\gamma_1 \sinh\nu_2\Delta z = 0$$

Substituting for ν_1 , the above equation can be shown to become :

$$\tan wz_1\gamma_1 = \frac{\mu_2\gamma_2}{\mu_1\gamma_1} \quad \frac{\mu_2\gamma_2 \tanh \nu_2\Delta z + \mu_3\gamma_3}{\mu_3\gamma_3 \tanh \nu_2\Delta z + \mu_2\gamma_2}$$

The equation for a layer over a half-space is :

$$\tan wz_1\gamma_1 = \frac{\mu_2\gamma_2}{\mu_1\gamma_1}$$

Comparing the above equation with the previous one, we see that the only difference is the multiplicative function on the right handside in the previous equation. The multiplicative function is a positive monotone function over the range of c under consideration. Thus the two equations have the same number of zeros. Aki & Richards (1980) have shown the number of modes entering at a given w, is :

$$n = \frac{wz}{\pi\beta_1}\left(1 - \frac{\beta_1^2}{\beta_2^2}\right)^{\frac{1}{2}} \qquad \text{(A1)}$$

Case 2: $\beta_2 < c < \beta_3$

$$\nu_1 = iw\gamma_1, \; \nu_2 = iw\gamma_2, \; \gamma_2 = \sqrt{\frac{1}{\beta_2^2} - \frac{1}{c^2}}, \; \nu_3 = w\gamma_3$$

where γ_1 and γ_3 have the same definitions as for Case 1.

It can be shown that $g = 0$ implies that :

$$\tan w\Delta z\gamma_2 = \frac{\mu_2\gamma_2\,[\mu_3\gamma_3-\mu_1\gamma_1 \tan wz_1\gamma_1]}{\mu_2^2\gamma_2^2+\mu_1\mu_3\gamma_1\gamma_3 \tan wz_1\gamma_1}$$

The solution of the above equation gives us another set of modes, only those that are continuous at $c = \beta_2$ and connects with the modes in the upper layer are permissible. Therefore the number of modes does not change and remains the same that we discussed in Case 1.

It remains to show that the zeros of g are not zeros of f. We will give the results next for $f = 0$ with notations and definitions given in Cases 1 & 2 previously.

b) Zeros of f:

Case 1: $\beta_1 < c < \beta_2$ $f(w,k) = 0$ implies that :

$$\tan wz_1\gamma_1 = \frac{-\mu_1\gamma_1}{\mu_2\gamma_2}\;\frac{\mu_3\gamma_3 \tanh\nu_2\Delta z+\mu_2\gamma_2}{\mu_2\gamma_2 \tanh\nu_2\Delta z+\mu_3\gamma_3}$$

Clearly the zeros of the above equation are different from those for $g = 0$ (Case 1) that we discussed previously.

Case 2: $\beta_2 < c < \beta_2$ $f(w,k) = 0$ implies that :

$$\tan w\gamma_2\Delta z = \frac{\mu_2\gamma_2[\mu_3\gamma_3+\mu_1\gamma_1 \cot w\gamma_1 z_1]}{\mu_2^2\gamma_2^2-\mu_1\mu_3\gamma_1\gamma_3 \cot w\gamma_1 z_1}$$

Again the zeros of the above equation are clearly different from those for $g = 0$ (Case 2).

To compute the zeros of $g = 0$, at any given w, we can compute the zeros for the problem of a layer over a half space. The properties of the half-space are the same as those of the second layer in our model and those for the surface layer is the same in the two models. We then use the obtained value k_j as initial value for Newton-Raphson iteration on $g(w,k)$ to find the refined root k'_j for our problem. We then factor out the root and repeat the procedure to synthesize the rest of the roots. A simple program to compute the total number of roots that are required shows that for the 2048 frequence samples that are required the total number of roots reaches tens of thousands. The number of roots entering the solution at any value of w, increases linearly with w. As the roots are independent of the station location x, and they are expensive to compute it is recommended to compute them once and store them for subsequent usage.

Since each pole is a simple pole, the residue of $e^{-ikx}F$ at the root k'_j can be given by :

$$e^{-ik'_j x} \frac{f(w,k'_j)}{} \frac{1}{g'(w,k'_j)}, \quad g' = \frac{\partial g}{\partial k} .$$

Appendix III

Arrival Times of Important Phases

$$SO = \frac{x}{\beta_1}$$

$$S1 \quad 2\sqrt{\frac{h_1^2 + \frac{x^2}{4}}{\beta_1}}$$

$$S2 = 2 \cdot .2 \frac{1}{\beta_1}\left(\sqrt{h_1^2 + \left(\frac{x}{2.2}\right)^2}\right)$$

$$\vdots$$

$$SN = 2N \frac{1}{\beta_1}\left(\sqrt{h_1^2 + \left(\frac{x}{2N}\right)^2}\right)$$

$$SC = \frac{x}{\beta_2} + 2h_1\sqrt{\frac{\beta_2^2 - \beta_1^2}{\beta_1\beta_2}}$$

$$RO \simeq 2\left(\frac{h_1}{\beta_1} + \frac{2h_2}{\beta_2} + \frac{x^2}{4[h_1\beta_1 + h_2\beta_2]}\right); \left|\frac{x}{h_1 + h_2}\right| << 1$$

$$R1 \simeq RO + \frac{2h_1}{\beta_1}$$

$$R2 \simeq RO + \frac{4h_1}{\beta_1}$$

$$\vdots$$

$$RN \simeq RO + 2N\frac{h_1}{\beta_1}$$

Table 1

Arrival Times of Important Phases (in second)

Station Location	X(km)	.2	.3	.4
Direct Arrival	S0	.500	.750	1.000
1st Multiple	S1	.707	.901	1.118
2nd Multiple	S2	1.118	1.250	1.414
	S3	1.581	1.677	1.803
	S4	2.062	2.136	2.236
	S5	2.550	2.610	2.693
	S6	3.041	3.092	3.162
	S7	3.536	3.579	3.640
	S8	4.031	4.070	4.123
	S9	4.528	4.562	4.610
	S10	5.025	5.056	5.099
	S11	5.523	5.551	5.590
	S12	6.021	6.047	6.083
	S13	6.519	6.543	6.576
	S14	7.018	7.040	7.071
	S15	7.517	7.537	7.566
Critical Wave	SC	.554	.582	.611
Deep Reflection	R0	3.301	3.301	3.302
1st Multiple	R1	3.801	3.801	3.802
2nd Multiple	R2	4.301	4.301	4.302
	R3	4.801	4.801	4.802
	R4	5.301	5.301	5.302
	R5	5.801	5.801	5.802
	R6	6.301	6.301	6.302
	R7	6.801	6.801	6.802
	R8	7.301	7.301	7.302
	R9	7.801	7.801	7.802

FIG. 3

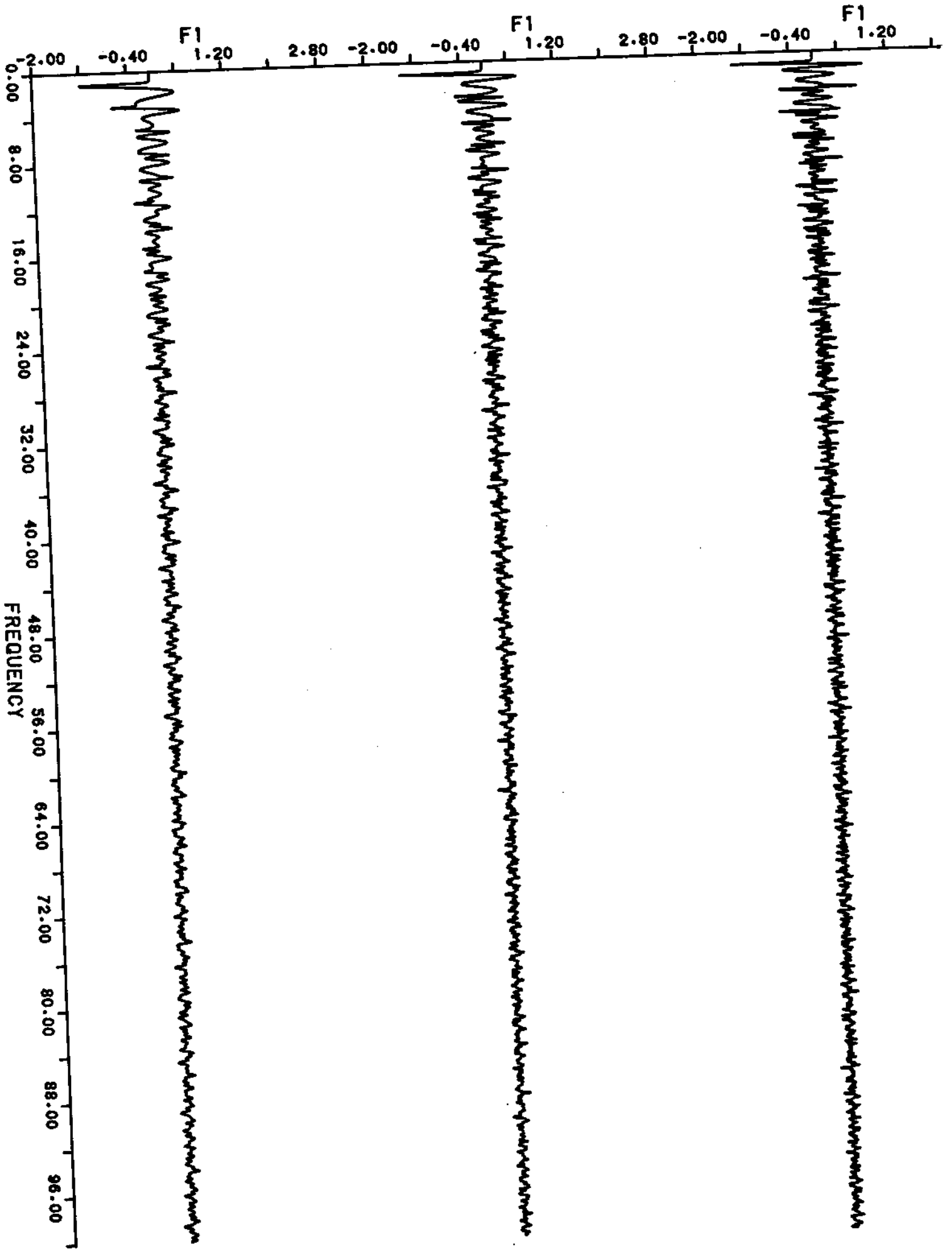
F1
-2.00
-0.40
1.20
2.80
-2.00
-0.40
1.20
2.80
-2.00
-0.40
1.20
0.00
8.00
16.00
24.00
32.00
40.00
48.00
56.00
64.00
72.00
80.00
88.00
96.00
FREQUENCY

FIG. 4

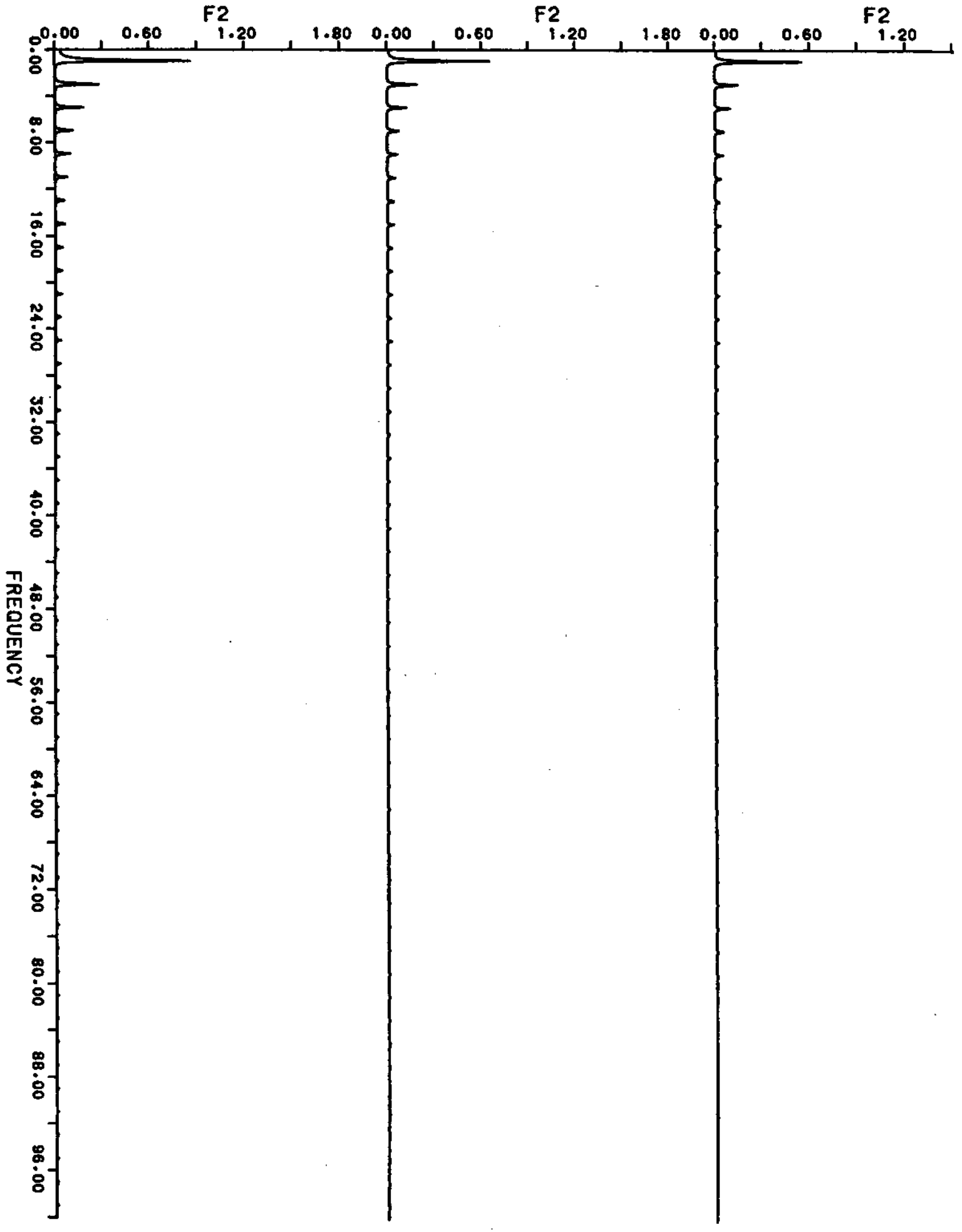
F2
0.00
0.60
1.20
1.80
F2
0.00
0.60
1.20
1.80
F2
0.00
0.60
1.20
FREQUENCY
0.00
8.00
16.00
24.00
32.00
40.00
48.00
56.00
64.00
72.00
80.00
88.00
96.00

FIG. 5

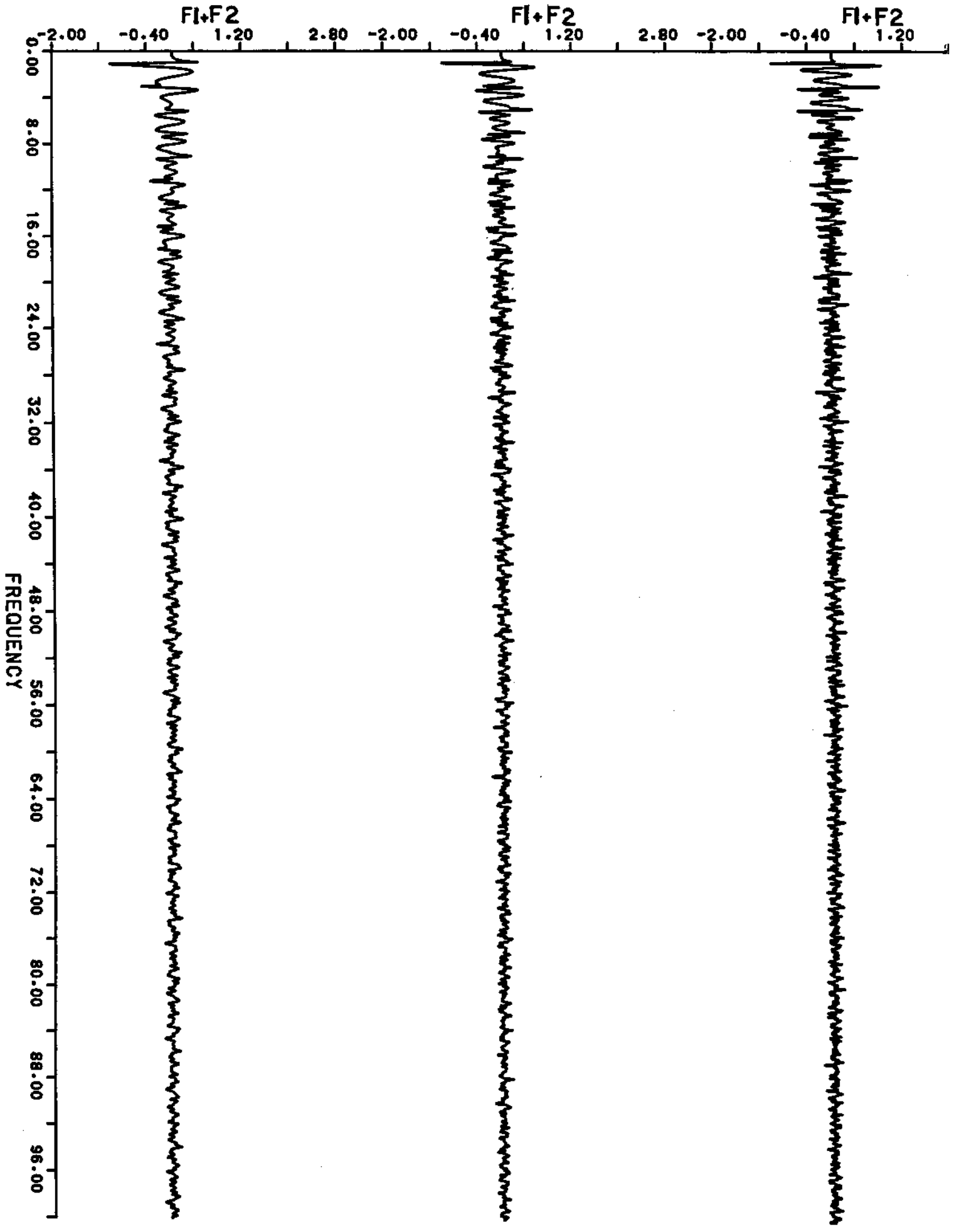
F1+F2
-2.00
-0.40
1.20
2.80
F1+F2
-2.00
-0.40
1.20
2.80
F1+F2
-2.00
-0.40
1.20
0.00
8.00
16.00
24.00
32.00
40.00
48.00
56.00
64.00
72.00
80.00
88.00
96.00
FREQUENCY

FIG. 6

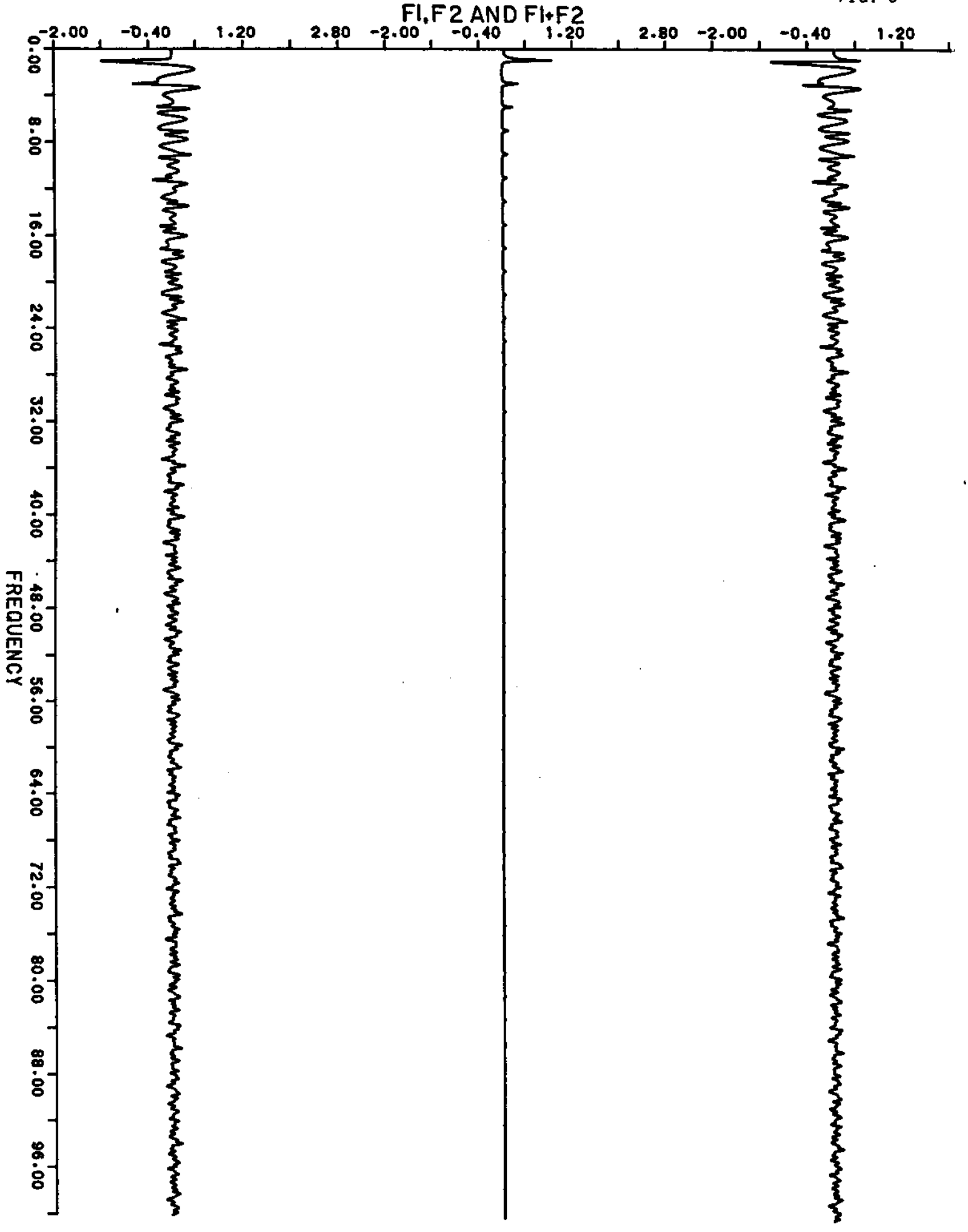
F1,F2 AND F1+F2
-2.00
-0.40
1.20
2.80
-2.00
-0.40
1.20
2.80
-2.00
-0.40
1.20
0.00
8.00
16.00
24.00
32.00
40.00
48.00
56.00
64.00
72.00
80.00
88.00
96.00
FREQUENCY

FIG. 7

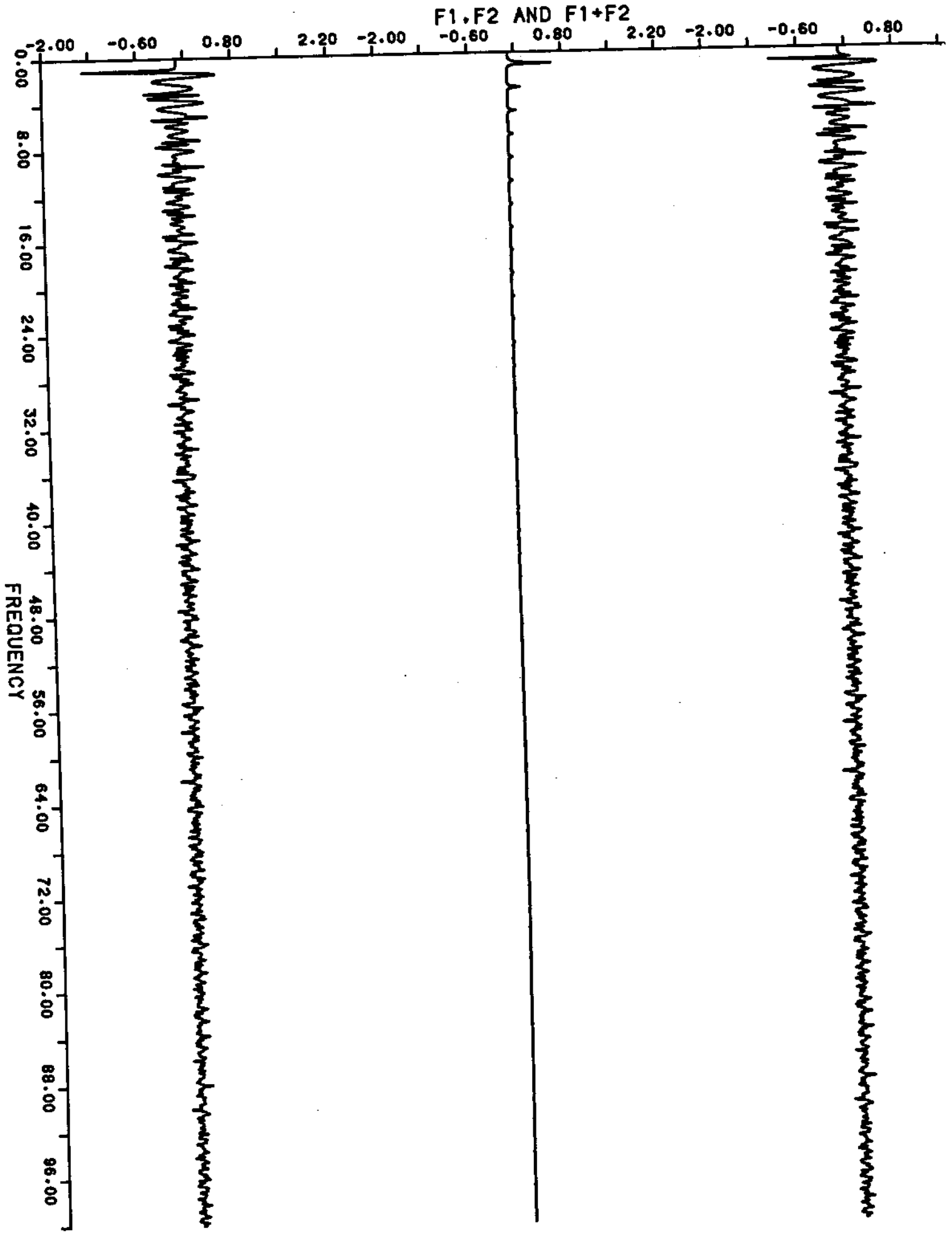
F1,F2 AND F1+F2
-2.00
-0.60
0.80
2.20
-2.00
-0.60
0.80
2.20
-2.00
-0.60
0.80
0.00
8.00
16.00
24.00
32.00
40.00
48.00
56.00
64.00
72.00
80.00
88.00
96.00
FREQUENCY

FIG. 8

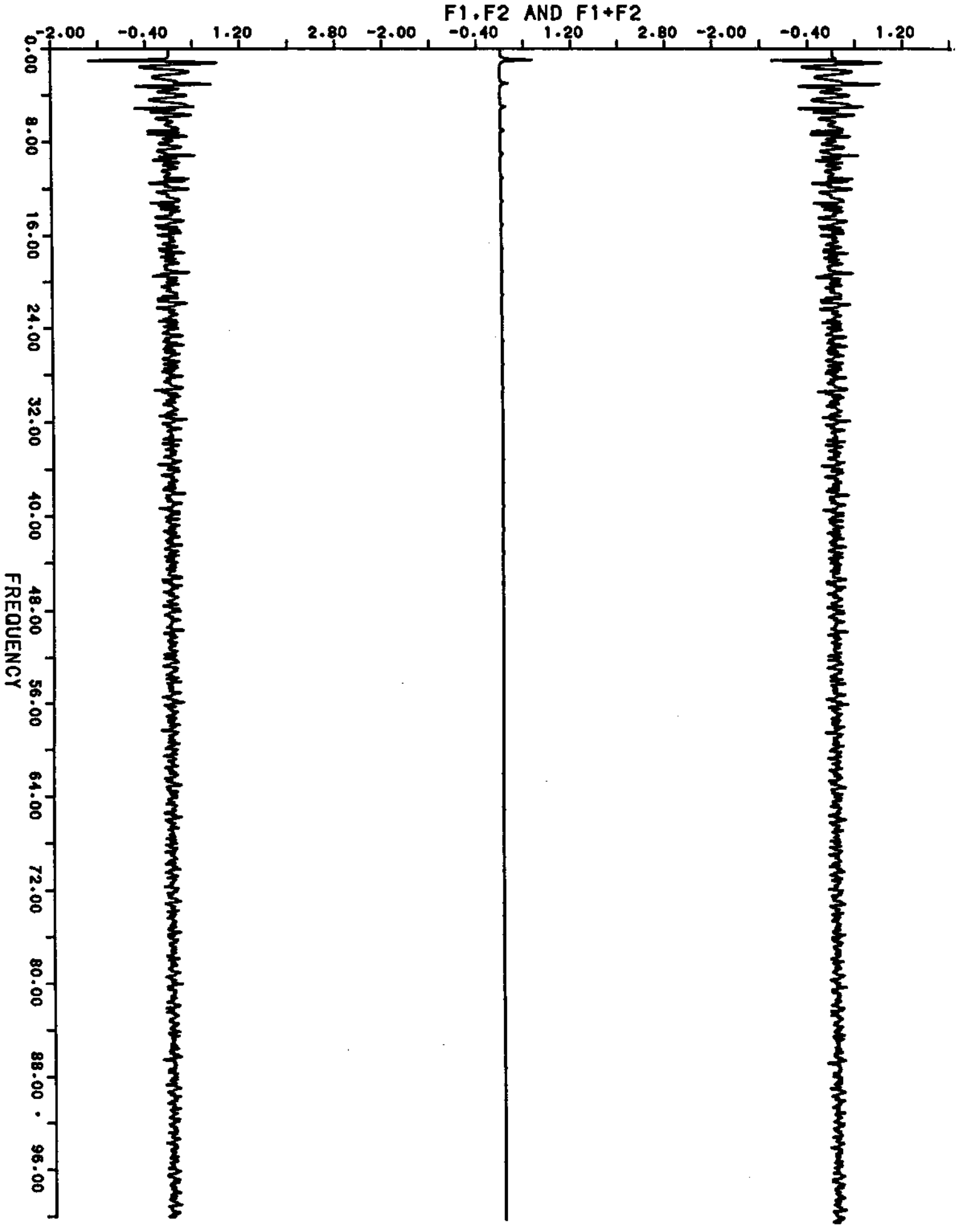
F1,F2 AND F1+F2
-2.00
-0.40
1.20
2.80
-2.00
-0.40
1.20
2.80
-2.00
-0.40
1.20
0.00
8.00
16.00
24.00
32.00
40.00
48.00
56.00
64.00
72.00
80.00
88.00
96.00
FREQUENCY

FIG. 9

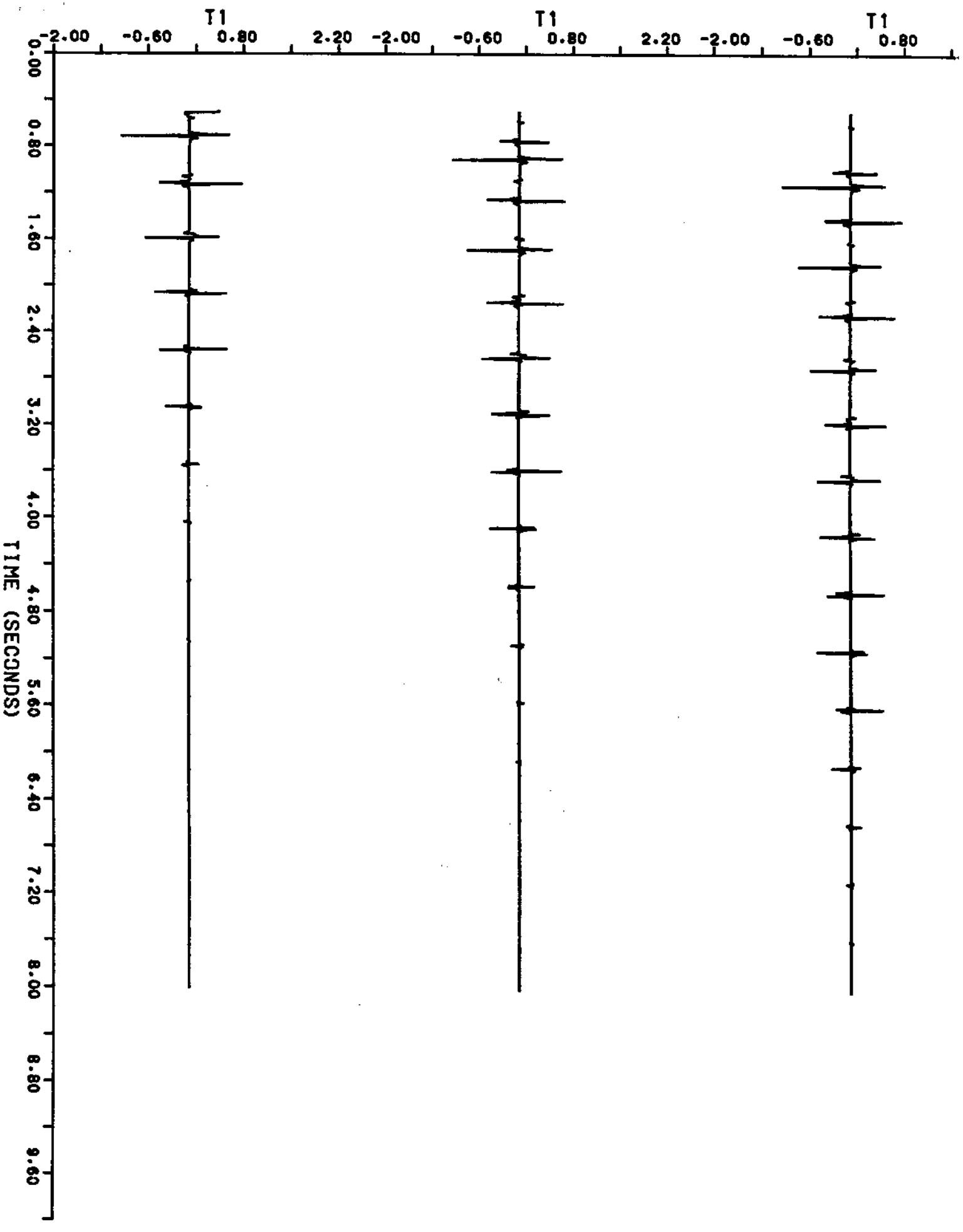
T1
-2.00
-0.60
0.80
2.20
T1
-2.00
-0.60
0.80
2.20
T1
-2.00
-0.60
0.80
0.00
0.80
1.60
2.40
3.20
4.00
4.80
5.60
6.40
7.20
8.00
8.80
9.60
TIME (SECONDS)

FIG. 10

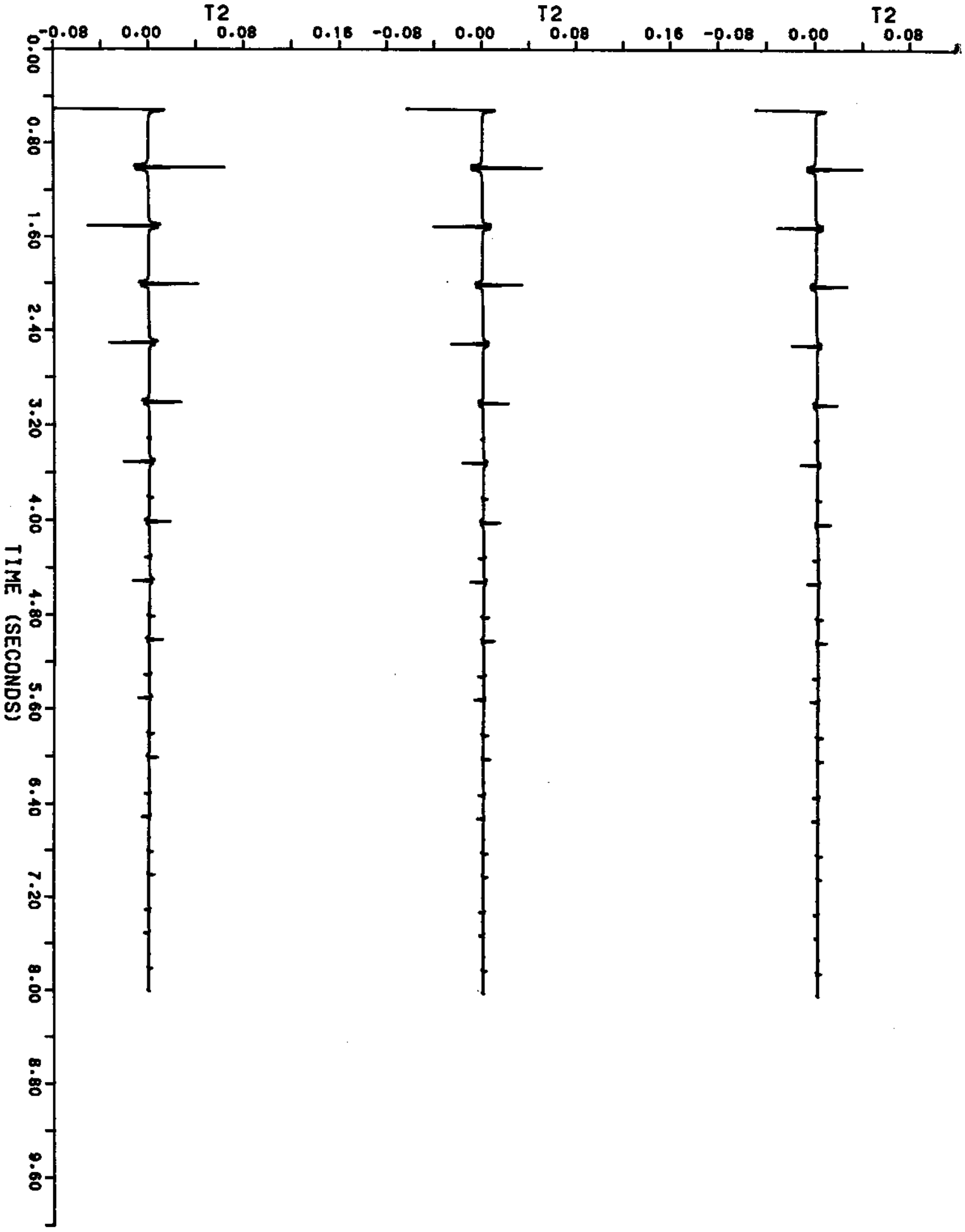
T2
-0.08
0.00
0.08
0.16
T2
-0.08
0.00
0.08
0.16
T2
-0.08
0.00
0.08
0.00
0.80
1.60
2.40
3.20
4.00
4.80
5.60
6.40
7.20
8.00
8.80
9.60
TIME (SECONDS)

FIG. 11

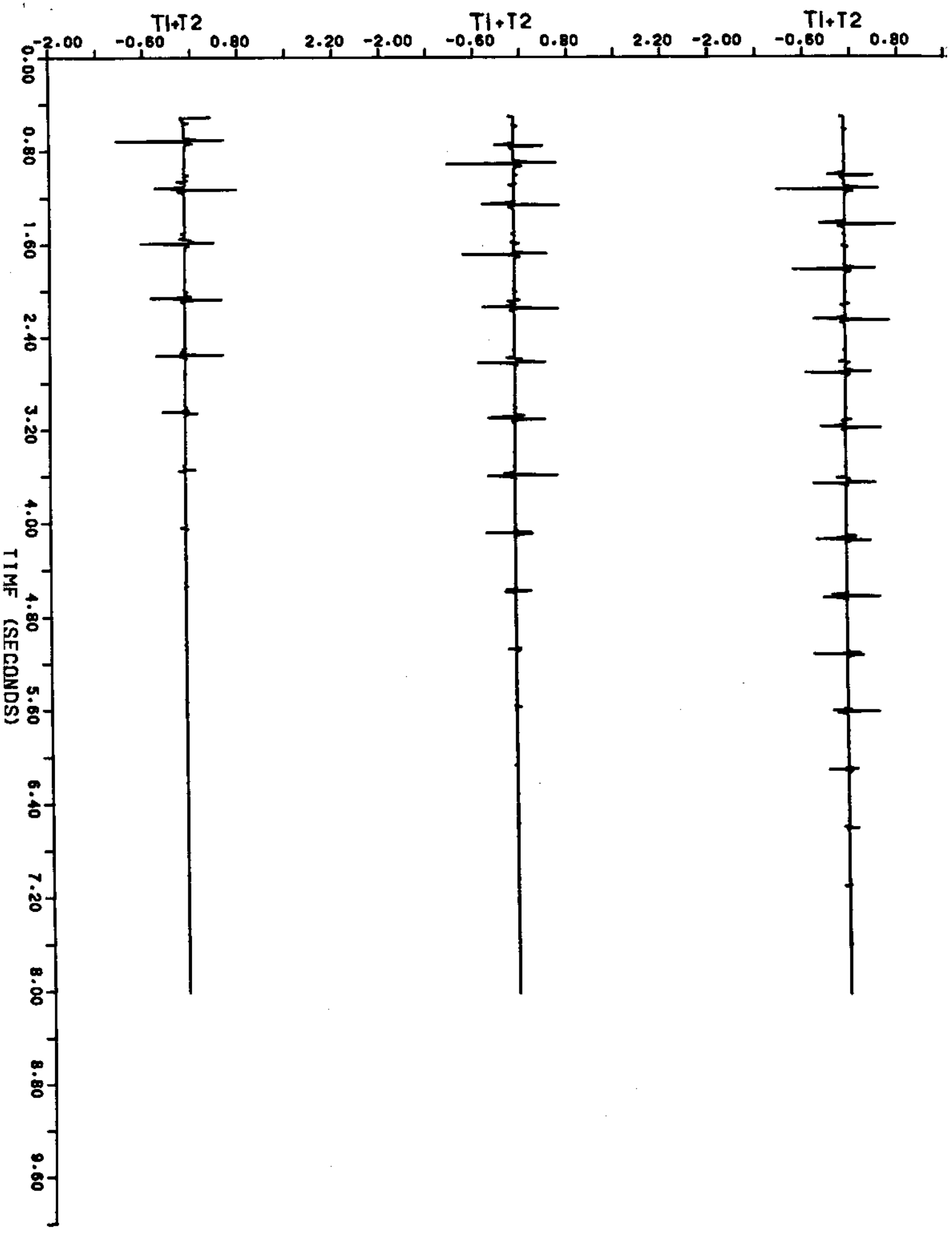
T1+T2
-2.00
-0.60
0.80
2.20
T1+T2
-2.00
-0.60
0.80
2.20
T1+T2
-2.00
-0.60
0.80
0.00
0.80
1.60
2.40
3.20
4.00
4.80
5.60
6.40
7.20
8.00
8.80
9.60
TIME (SECONDS)

FIG. 12

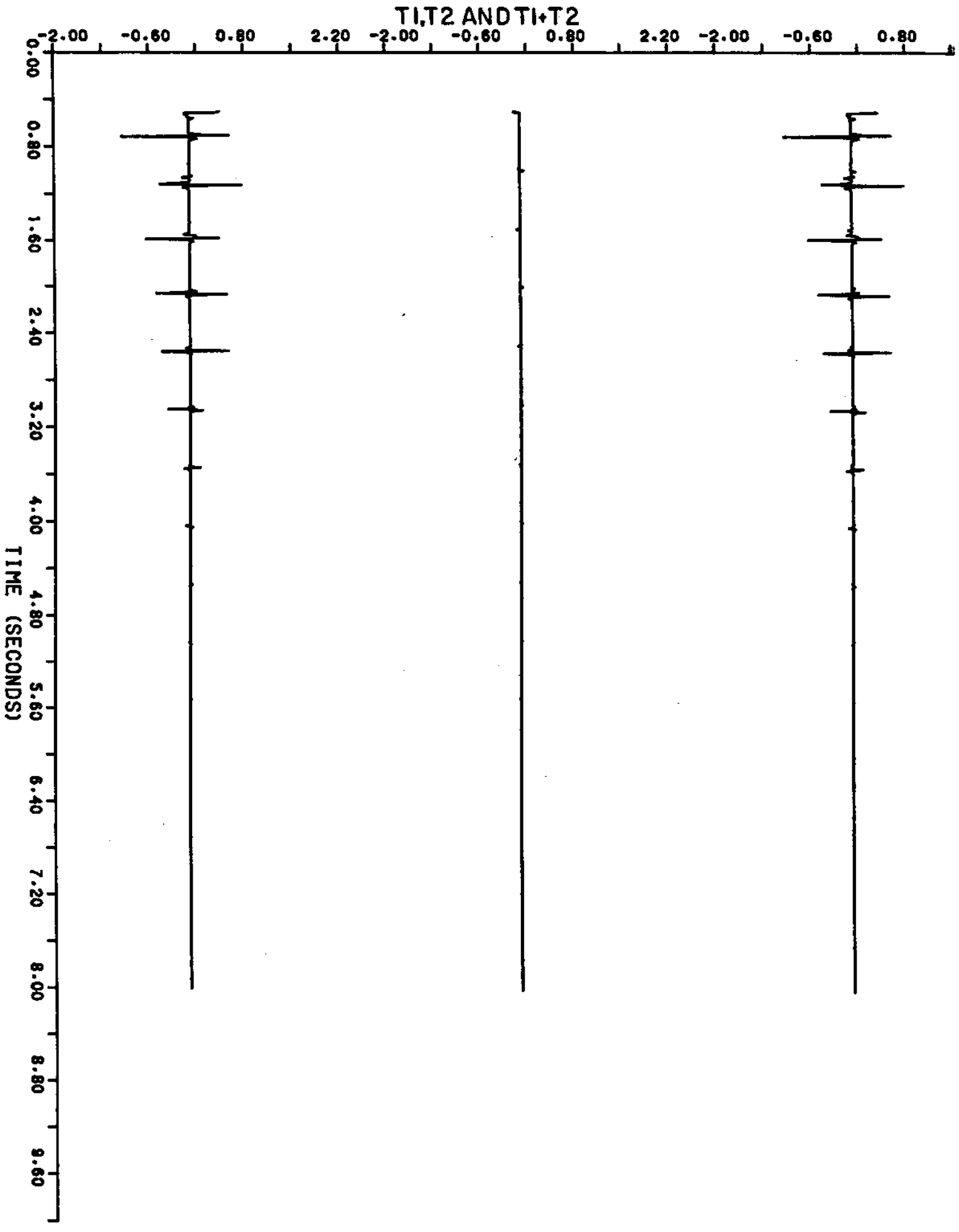
T1,T2 AND T1+T2
-2.00
-0.60
0.80
2.20
-2.00
-0.60
0.80
2.20
-2.00
-0.60
0.80
0.00
0.80
1.60
2.40
3.20
4.00
4.80
5.60
6.40
7.20
8.00
8.80
9.60
TIME (SECONDS)

FIG. 13

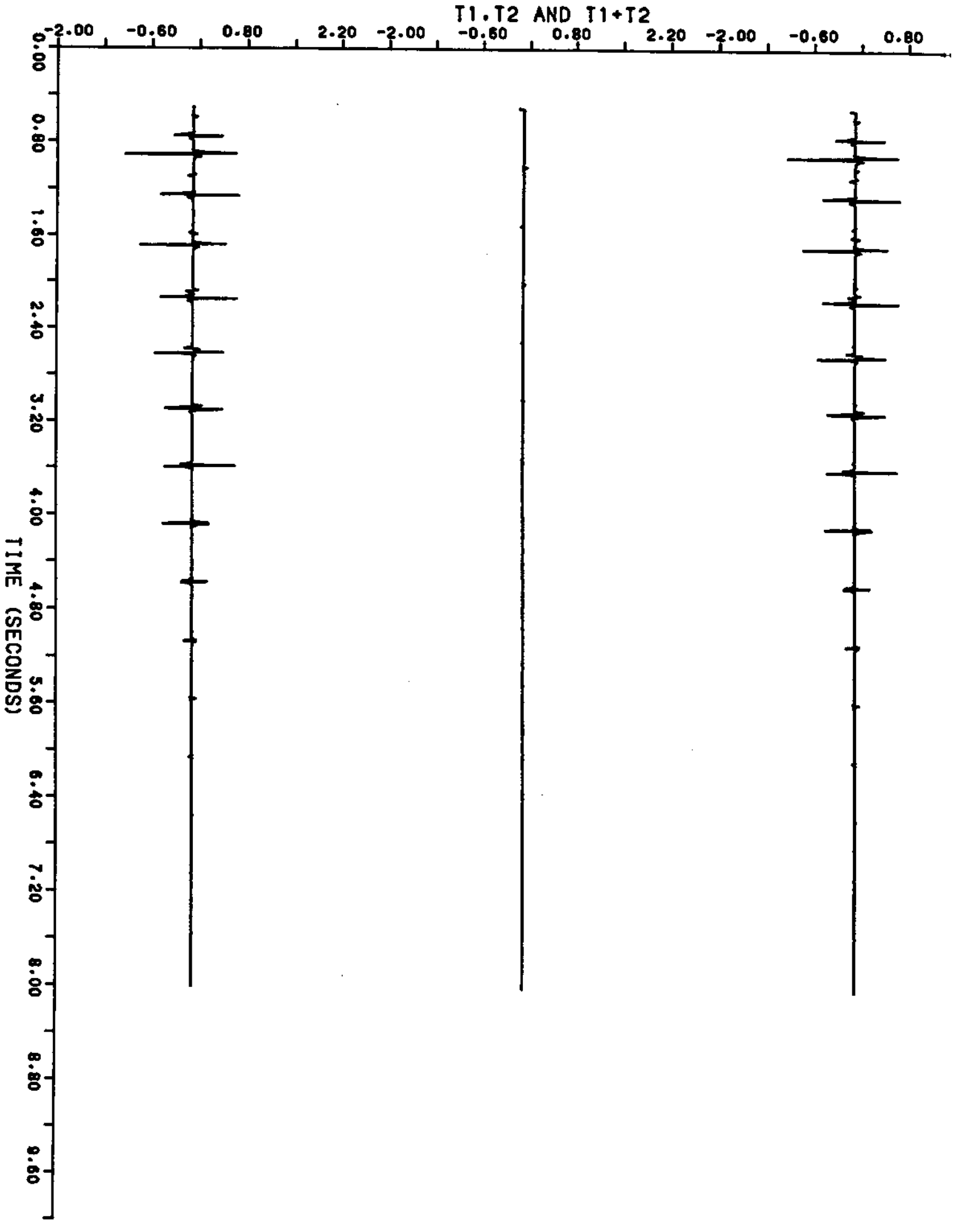
T1.T2 AND T1+T2
-2.00
-0.60
0.80
2.20
-2.00
-0.60
0.80
2.20
-2.00
-0.60
0.80
0.00
0.80
1.60
2.40
3.20
4.00
4.80
5.60
6.40
7.20
8.00
8.80
9.60
TIME (SECONDS)

FIG. 14

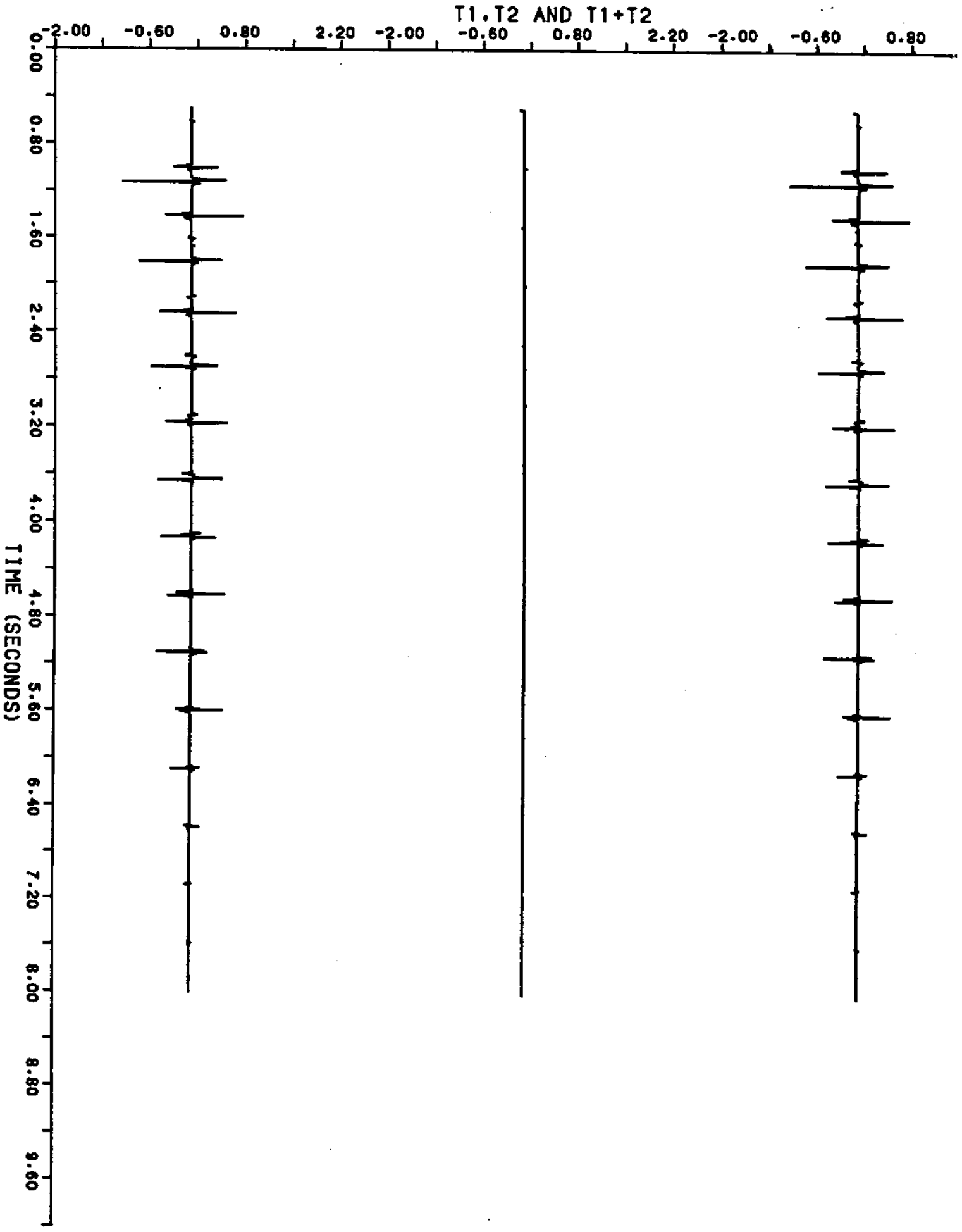
T1, T2 AND T1+T2
-2.00
-0.60
0.80
2.20
-2.00
-0.60
0.80
2.20
-2.00
-0.60
0.80
0.00
0.80
1.60
2.40
3.20
4.00
4.80
5.60
6.40
7.20
8.00
8.80
9.60
TIME (SECONDS)

FIG. 15

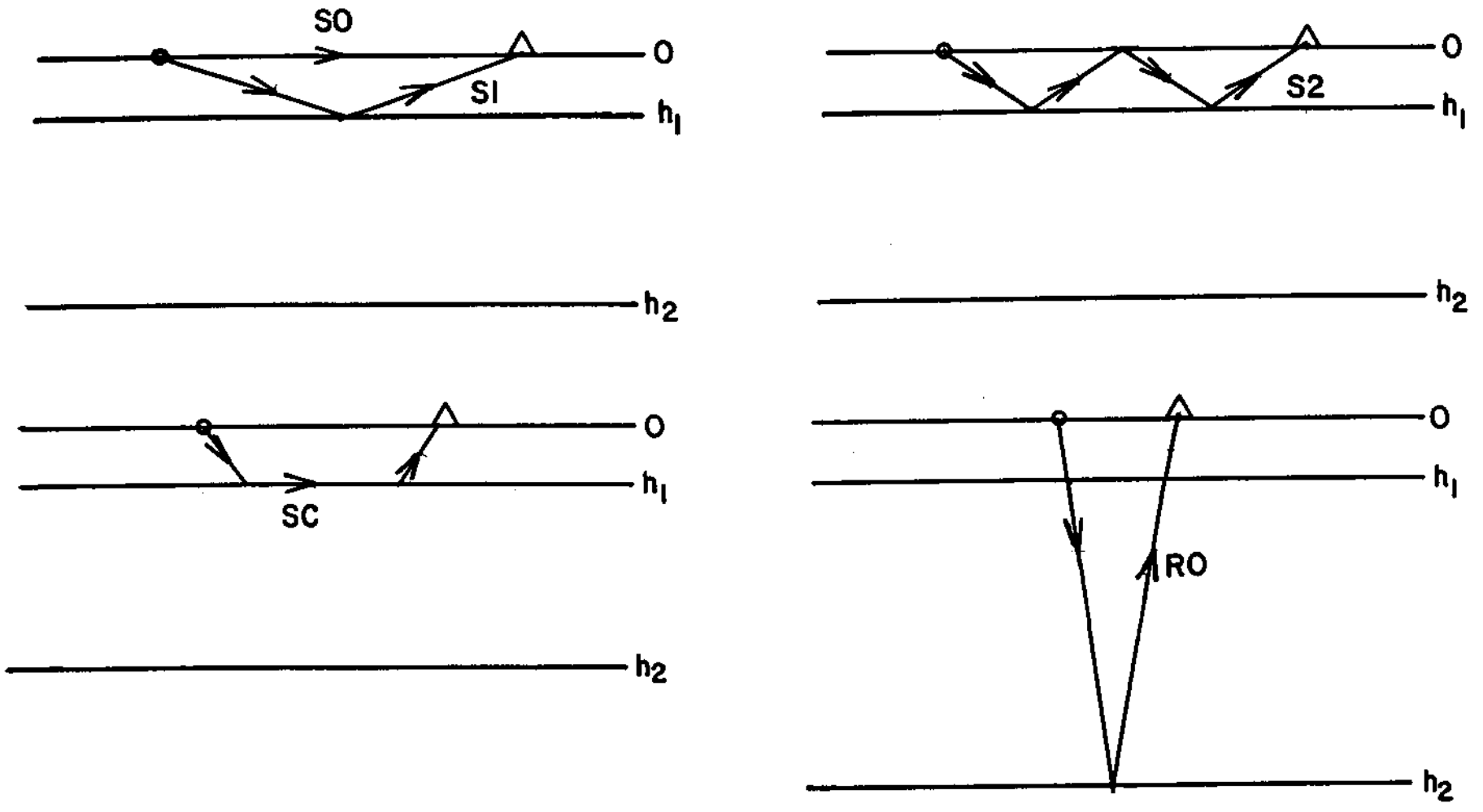

o : source

△ : station

FIG. 16

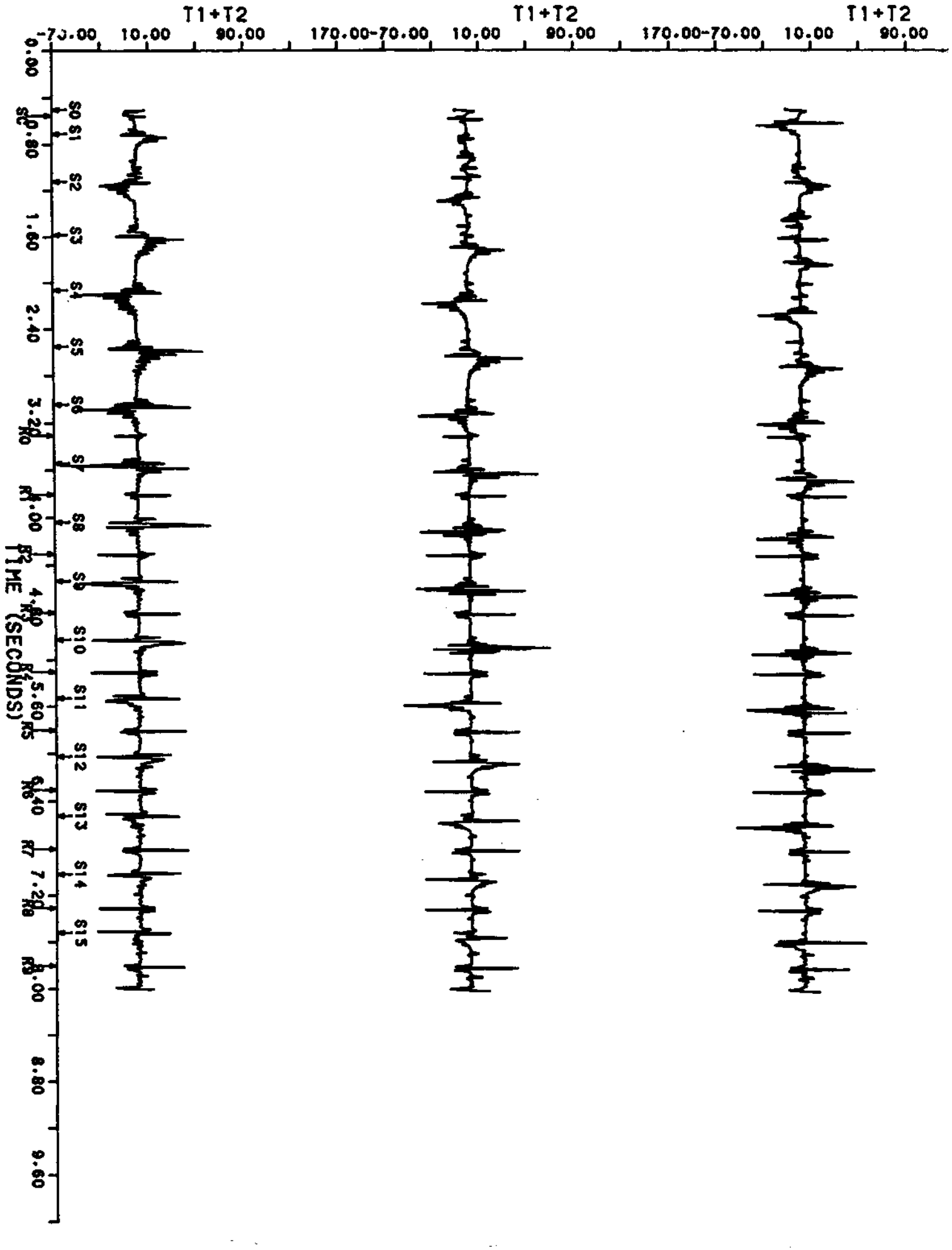
T1+T2
T1+T2
T1+T2
-70.00
10.00
90.00
170.00
-70.00
10.00
90.00
170.00
-70.00
10.00
90.00
0.00
0.80
1.60
2.40
3.20
4.00
4.80
5.60
6.40
7.20
8.00
8.80
9.60
S0
S1
S2
S3
S4
S5
S6
S7
S8
S9
S10
S11
S12
S13
S14
S15
R1
R2
R3
R4
R5
R6
R7
R8
TIME (SECONDS)